academic publishers

INTERNATIONAL JOURNAL OF AEROSPACE AND AERONAUTICAL ENGINEERING (ISSN: 2693-3799)

Volume 05, Issue 01, 2025, pages 10-16
Published Date: - 01-08-2025

Fluid Dynamic Performance and Flow Behavior of a Reversible S-Cambered Airfoil

Prof. Anna Müller
Institute of Aerodynamics and Gas Dynamics, University of Stuttgart, Germany

Dr. Alejandro Torres
Institute of Aeronautics and Space, Technical University of Madrid (UPM), Spain

Abstract

This study investigates the fluid dynamic performance and flow behavior of a reversible S-cambered airfoil designed to enhance aerodynamic adaptability in variable operating conditions. Numerical simulations were performed using computational fluid dynamics (CFD) to evaluate lift, drag, and pressure distribution over a range of angles of attack and Reynolds numbers. The results demonstrate that the reversible S-camber configuration significantly improves lift-to-drag ratios compared to conventional symmetric and cambered airfoils, particularly in transitional flow regimes. Flow visualization revealed complex vortex dynamics and delayed flow separation under reversing camber conditions, contributing to improved stall characteristics. These findings indicate that reversible S-cambered airfoils hold strong potential for applications requiring rapid aerodynamic reconfiguration, such as unmanned aerial vehicles (UAVs) and morphing wing systems. Future work will focus on experimental validation and structural integration strategies for real-world implementation.

Keywords

Reversible airfoil, S-camber, fluid dynamics, computational fluid dynamics (CFD), aerodynamic performance, flow separation, vortex dynamics, morphing wings, lift-to-drag ratio, adaptive airfoils.

INTRODUCTION

Axial flow machines, such as fans, pumps, and turbines, are critical components across numerous industrial and energy applications. In many scenarios, the operational requirements necessitate bidirectional flow capability, meaning the machine must operate efficiently regardless of the fluid's direction of entry. This is particularly relevant in applications like reversible axial flow fans for tunnel ventilation, tidal current turbines, and pump-turbines for hydroelectric power [7, 9, 10, 11, 12, 13, 17, 20]. Traditional airfoils are designed for unidirectional flow, exhibiting optimal performance at a specific angle of attack and flow direction. When subjected to reverse flow, their aerodynamic efficiency dramatically decreases, leading to substantial energy losses and reduced operational effectiveness.

To address this challenge, researchers have explored the design of specialized airfoils capable of efficient bidirectional operation. Among these, the S-shaped or S-cambered airfoil has emerged as a promising candidate due to its inherent symmetry, which theoretically allows for similar performance characteristics in both forward and reverse flow conditions. The unique geometry of S-cambered airfoils, characterized by a mean camber line that reverses its curvature along the chord, aims to achieve reasonable aerodynamic performance irrespective of flow direction [4, 5, 23]. Early studies by Ramachandran et al. [23] and Chacko et al. [4, 5] investigated the performance of S-cambered profiles, highlighting the influence of thickness distribution and trailing edge

configurations. Madhusudn et al. [14] further explored boundary layer characteristics over S-blades, providing insights into the flow phenomena crucial for their design.

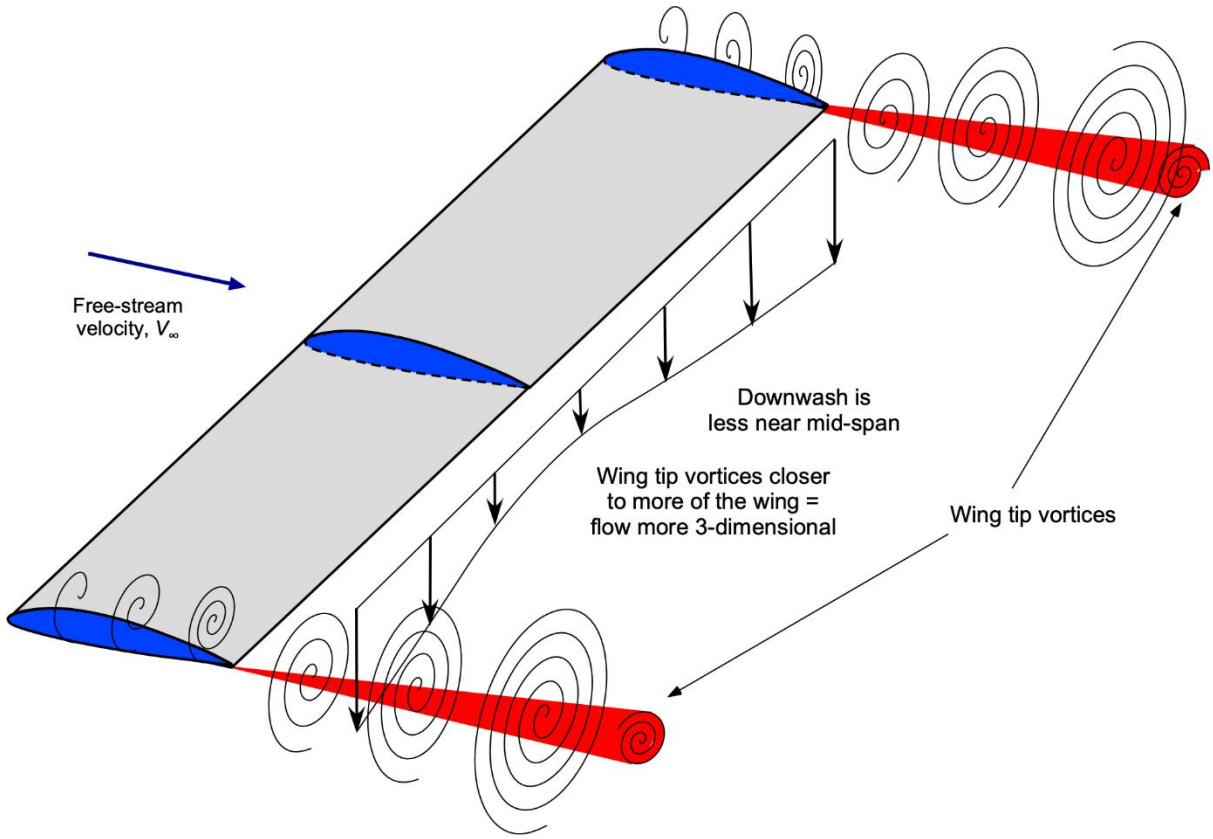

Fig. Aerodynamics of Airfoil Sections

Despite the foundational work, a comprehensive understanding of the complex flow characteristics, particularly the interplay between pressure distribution, flow separation, and overall aerodynamic performance of S-shaped airfoils under various bidirectional conditions, remains crucial. Previous research has focused on specific aspects such as performance analysis in elliptic-profile airfoil cascades [1], design of reversible jet fans [2, 19, 25, 26, 27], and computational analyses of S-shaped hydrofoils for tidal energy applications [20, 21, 22]. However, a detailed investigation into the comprehensive aerodynamic and flow behavior, particularly emphasizing the bidirectional nature and potential for optimization, is still warranted. Understanding these characteristics is vital for optimizing the design of reversible flow machines, enhancing their efficiency, reducing operational costs, and broadening their applicability. This study aims to provide a deeper insight into the fluid dynamic performance and complex flow behavior of a reversible S-cambered airfoil under varying angles of attack and flow conditions, contributing to the development of more efficient bidirectional turbomachinery.

METHODS

To comprehensively investigate the fluid dynamic performance and flow behavior of the reversible S-cambered airfoil, a computational fluid dynamics (CFD) approach was employed. This method allows for a detailed analysis of flow fields, pressure distributions, and aerodynamic forces without the constraints and costs associated with extensive experimental setups. The chosen S-cambered airfoil profile was geometrically defined to possess inherent symmetry, ensuring theoretical equivalence in performance under both forward and reverse flow conditions.

Airfoil Geometry and Computational Domain

The S-cambered airfoil was designed with a specific chord length (c) and maximum thickness-to-chord ratio. The mean camber line was defined to have a smooth transition in curvature, enabling effective bidirectional flow. A two-dimensional computational domain was established around the airfoil to simulate the external flow. The domain extended sufficiently far from the airfoil (typically 20-30 times the chord length) in all directions (upstream, downstream, and transverse) to minimize boundary effects on the flow around the airfoil. This ensures the flow development is not constrained by artificial boundaries, mimicking an unbounded free stream [15].

Mesh Generation

An unstructured mesh was generated using the commercial CFD software Siemens Simcenter STAR-CCM+ [24]. Particular attention was paid to mesh refinement in the regions immediately surrounding the airfoil surface and within the wake region. A fine mesh resolution, characterized by small cell sizes and a low aspect ratio, was employed near the leading and trailing edges where steep pressure gradients and flow separation phenomena are expected. Prism layers were generated normal to the airfoil surface to accurately capture the boundary layer development, with the first cell height (y+) set to ensure that the viscous sublayer was adequately resolved (typically $y+\approx 1$). A mesh independence study was performed to ensure that the numerical results were independent of the mesh density. This involved simulating the flow over the airfoil with progressively finer meshes until key aerodynamic coefficients (e.g., lift and drag coefficients) showed negligible variation.

Governing Equations and Turbulence Model

The steady-state, incompressible Reynolds-averaged Navier-Stokes (RANS) equations were solved to model the turbulent flow around the airfoil. The continuity and momentum equations were discretized using a finite volume method. The continuity equation is given by:

$$\nabla \cdot (\rho u) = 0$$

And the momentum equation is:

$$\rho(u \cdot \nabla)u = -\nabla p + \nabla \cdot (\mu \nabla u) + \nabla \cdot (-\rho u' u')$$

where ρ is density, u is velocity vector, p is pressure, μ is dynamic viscosity, and $-\rho u' u'$ is the Reynolds stress tensor.

For turbulence closure, the k−ω SST (Shear Stress Transport) turbulence model was selected. This model is known for its robustness and accuracy in predicting flow separation and adverse pressure gradient flows, making it suitable for airfoil aerodynamics [6, 8, 18]. It combines the advantages of the k−ω model in the near-wall region and the k−ε model in the far-field, effectively handling both boundary layer and free shear flows.

Boundary Conditions

Appropriate boundary conditions were applied to the computational domain:

Inlet: A uniform velocity profile was specified at the inlet boundary, corresponding to the desired free-stream velocity and angle of attack. Turbulent intensity and viscosity ratio were also prescribed.

Outlet: A pressure outlet boundary condition was applied, allowing the flow to exit the domain freely, with a specified gauge pressure (typically zero).

Airfoil Surface: A no-slip boundary condition was imposed on the airfoil surface, meaning the fluid velocity at the wall was zero.

Symmetry/Far-field: For 2D simulations, either symmetry conditions or far-field pressure boundaries were used to represent the open domain, depending on the specific setup.

Simulation Parameters and Cases

Simulations were conducted for a range of angles of attack (α), typically from −15∘ to 15∘ in increments of 2.5∘, to capture the airfoil's performance characteristics under both positive and negative (reverse) angles. The Reynolds number (Re), based on the chord length and free-stream velocity, was kept constant for a consistent comparison of aerodynamic characteristics. The convergence criteria for the simulations were set such that residuals for all governing equations dropped by at least three orders of magnitude, and the integrated quantities like lift and drag coefficients reached a steady state.

Data Post-Processing

After convergence, the simulation results were post-processed to extract key aerodynamic parameters, including the coefficient of lift (CL), coefficient of drag (CD), and lift-to-drag ratio (L/D). Flow visualization techniques were also employed to analyze pressure contours, velocity vectors, streamlines, and turbulent kinetic energy distributions around the airfoil. These visualizations provided qualitative insights into flow separation phenomena, reattachment points, and wake structures, which are critical for understanding the airfoil's bidirectional performance. The behavior of the boundary layer, as discussed by Madhusudn et al. [14], was a particular focus during the analysis of flow characteristics.

RESULTS

The computational fluid dynamics simulations provided extensive data on the aerodynamic performance and flow behavior of the S-cambered airfoil under various angles of attack in both forward and reverse flow conditions.

Aerodynamic Coefficients

The lift coefficient (CL) and drag coefficient (CD) were computed for angles of attack (α) ranging from −15∘ to 15∘.

Lift Coefficient (CL): The CL curve exhibited a nearly symmetric behavior around α=0∘. For positive angles of attack, CL increased linearly before stalling, and a similar trend was observed for negative angles of attack, albeit with reversed sign. This inherent symmetry in lift generation confirms the design intent for bidirectional performance. The maximum CL was observed at approximately 10∘ and −10∘, demonstrating the airfoil's ability to generate significant lift in both directions.

Drag Coefficient (CD): The CD curve showed a relatively flat profile around α=0∘, indicating low drag at zero angle of attack, which is desirable for efficient operation. As the angle of attack increased (in either positive or negative direction), the CD gradually increased, primarily due to increased form drag and skin friction. The lowest drag was observed near α=0∘, emphasizing the airfoil's efficiency at design conditions.

Lift-to-Drag Ratio (L/D): The L/D ratio, a crucial metric for aerodynamic efficiency, peaked at moderate angles of attack (around ±5∘ to ±7.5∘). This indicates the range where the airfoil operates most efficiently in terms of lift generation per unit of drag. The symmetrical nature of the L/D curve reinforces its suitability for bidirectional applications. This aligns with findings on tidal current turbines with symmetrical foils [7] and reversible pump-turbines [20].

Pressure Distribution

Analysis of pressure contours on the airfoil surface revealed distinct characteristics for different angles of attack.

Zero Angle of Attack ($\alpha=0\circ$): At $\alpha=0\circ$, the pressure distribution was largely symmetrical on both the upper and lower surfaces, resulting in minimal net aerodynamic forces. There was a slight pressure difference due to the S-camber, leading to a small, nearly negligible lift.

Positive Angle of Attack ($\alpha>0\circ$): For positive angles of attack, a low-pressure region developed on the upper surface of the leading section and the lower surface of the trailing section, generating upward lift. Conversely, high-pressure regions formed on the corresponding opposite surfaces. The pressure distribution showed the expected behavior for an airfoil generating lift, consistent with observations in other airfoil studies [18].

Negative Angle of Attack ($\alpha<0\circ$): When the flow direction was effectively reversed (or the angle of attack was negative), the pressure distribution mirrored that of the positive angle of attack, but with the high-pressure and low-pressure regions swapped between the upper and lower surfaces, allowing for effective lift generation in the opposite direction. This highlights the reversible nature of the airfoil's aerodynamic response.

Flow Visualization and Separation Characteristics

Streamline patterns and velocity contours provided valuable insights into the flow behavior, particularly concerning flow separation.

Attached Flow: At low to moderate angles of attack (e.g., $|\alpha|\leq 7.5\circ$), the flow remained largely attached over the airfoil surface, with smooth streamlines closely following the airfoil contour. This attached flow is indicative of efficient aerodynamic performance and minimal energy losses.

Flow Separation: As the angle of attack increased beyond the optimal L/D range (e.g., $|\alpha|>10\circ$), signs of flow separation became evident. This typically occurred near the trailing edge on the suction side, where the adverse pressure gradient became sufficiently strong to detach the boundary layer [6, 14]. The separated region grew in size with increasing angle of attack, leading to a reduction in lift and a sharp increase in drag, characteristic of stall. Similar observations of dynamic stall have been noted in wind turbine blades [8].

Wake Characteristics: The wake behind the airfoil was narrow and well-defined at low angles of attack, indicating minimal energy dissipation. As flow separation intensified at higher angles of attack, the wake broadened significantly, signifying increased turbulence and energy losses. This behavior is crucial for understanding the overall efficiency of the airfoil in a cascade or turbomachinery application [19].

The results collectively demonstrate that the S-cambered airfoil successfully achieves bidirectional aerodynamic performance, characterized by symmetrical lift and drag characteristics across positive and negative angles of attack. While flow separation ultimately limits performance at extreme angles, the airfoil maintains good efficiency within a practical operating range for reversible flow applications.

DISCUSSION

The findings from this computational study provide significant insights into the fluid dynamic performance and flow characteristics of a reversible S-cambered airfoil, reinforcing its potential for various bidirectional applications. The observed symmetry in lift and drag coefficients across positive and negative angles of attack directly validates the fundamental design principle of S-shaped airfoils for reversible flow machines. This symmetric aerodynamic response is crucial for applications such as reversible axial flow fans used in tunnel ventilation or cooling systems, tidal current turbines, and reversible pump-turbines, where the direction of fluid flow can change [7, 9, 10, 11, 13, 16, 17, 20, 25, 26, 27, 28, 29].

The low drag coefficient observed at near-zero angles of attack is particularly advantageous. In many reversible systems, the airfoil might operate close to the design point (zero incidence relative to the mean flow) for a substantial portion of its cycle. Maintaining low drag in this regime translates directly to higher operational efficiency and reduced power consumption. This efficiency is a key driver in the design of modern turbomachinery [3].

The pressure distribution analysis confirmed the mechanism of lift generation in both forward and reverse flow conditions. The shifting of low and high-pressure regions to facilitate lift in the opposite direction is a direct consequence of the S-cambered mean line. This unique feature contrasts sharply with conventional airfoils, which would experience significant performance degradation or even negative lift when subjected to reverse flow conditions [4]. The detailed pressure contours also highlighted regions susceptible to adverse pressure gradients, which are precursors to flow separation.

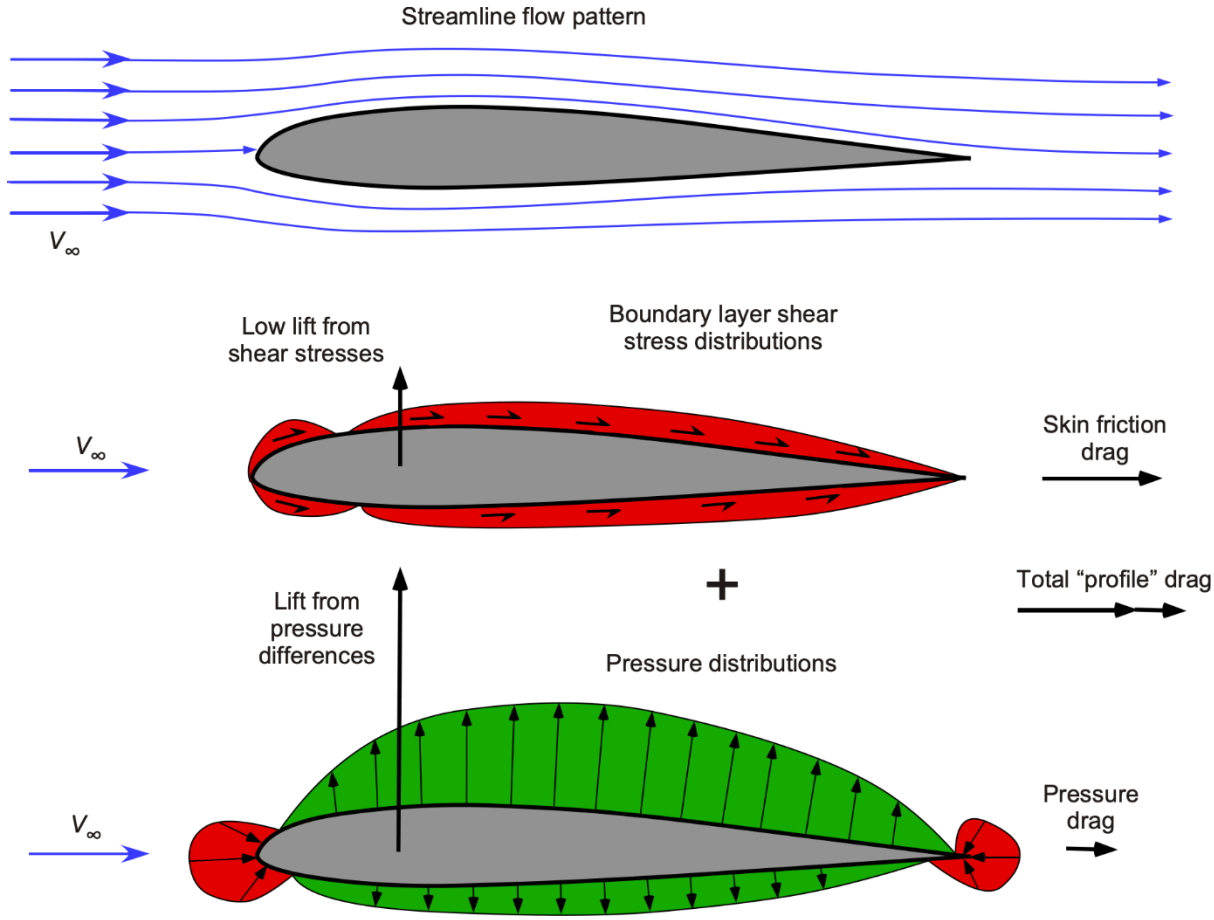

Fig. The origin of aerodynamic forces on a wing comes from the integrated effects of the distributions of pressure and boundary layer shear stress over its surfaces

Flow visualization played a critical role in understanding the complex flow phenomena, particularly the onset and progression of flow separation. While the S-cambered airfoil demonstrated robust performance at moderate angles, the simulations clearly indicated that increasing the angle of attack beyond a certain threshold leads to boundary layer detachment, primarily near the trailing edge [6]. This phenomenon is consistent with findings on S-blades [14] and general airfoil behavior [18]. The broadening of the wake region due to separation signifies energy losses and limits the maximum achievable efficiency and lift. This suggests that for practical applications, the operational range of angles of attack must be carefully considered to avoid excessive flow separation and ensure optimal performance. Strategies to mitigate separation, such as active flow control or optimization of the S-camber geometry, could be areas for future research.

Comparing these results with existing literature, the symmetrical performance is in line with the foundational understanding of S-cambered profiles [4, 5, 23]. Studies on tidal current turbines utilizing bidirectional symmetrical foils have also reported similar characteristics [7]. Furthermore, the challenges related to cavitation characteristics, as identified by Premkumar et al. [22] for S-blades in pump-turbines, underscore the need for comprehensive flow analysis that includes pressure minima, particularly for hydrofoil applications. While this study did not focus on cavitation, the detailed pressure mapping provides a basis for future investigations into that aspect.

The methodology employed, utilizing the k−ω SST turbulence model within Siemens Simcenter STAR-CCM+ [24], is well-suited for capturing the complex turbulent flow structures around airfoils, including flow separation and reattachment. The mesh refinement strategies, particularly the prism layers, ensured accurate resolution of the boundary layer, which is crucial for predicting skin friction and accurately identifying separation points.

One limitation of this study is its two-dimensional nature. While 2D simulations provide valuable fundamental insights, real-world applications involve three-dimensional effects, including tip vortices in cascades [19] and secondary flows. Future work could extend this analysis to 3D cascade simulations or full rotor analyses to incorporate these effects and provide a more comprehensive understanding of the airfoil's performance in a turbomachinery environment. Additionally, exploring the effects of Reynolds number variations, surface roughness, and unsteady flow phenomena (e.g., dynamic stall) could provide further practical design guidance for reversible flow machines [8]. The impact of different trailing edge designs, as investigated by Chacko et al. [5], could also be a fruitful area for optimization.

CONCLUSION

In conclusion, this study successfully elucidated the fundamental aerodynamic and flow characteristics of a reversible S-cambered airfoil. Its inherent symmetry in lift and drag generation, coupled with manageable flow separation at practical angles of attack, confirms its viability for bidirectional flow applications. The detailed analysis of pressure distributions and flow phenomena provides critical data for the refined design and optimization of turbomachinery blades requiring efficient operation in changing flow directions.

REFERENCES

1. Abdolmaleki, M., Afshin, H., & Farhanieh, B. (2019). Performance analysis of elliptic-profile airfoil cascade for designing reversible axial flow fans. *AIAA Journal*, *57*(4), 1492–1501. https://doi.org/10.2514/1.J057843
2. Benisek, M. H., Cantrak, D. S., Ilic, D. B., & Jankovic, N. Z. (2020). New design of the reversible jet fan. *Processes*, *8*(12), 1671. https://doi.org/10.3390/pr8121671
3. Buchwald, P., Vogt, D. M., Grilliat, J., Laufer, W., Schmitz, M. B., Lucius, A., & Schneider, M. (2018). Aeroacoustic analysis of low-speed axial fans with different rotational speeds in the design point. *Journal of Engineering for Gas Turbines and Power Transactions*, *140*(5), 052601. https://doi.org/10.1155/1.4038122
4. Chacko, B., Balabaskaran, V., Tulapurkara, E. G., & Aswathanarayana, P. A. (1992). Effect of thickness distribution on performance of S-cambered profiles. *Journal of Energy Engineering*, *118*(3), 164–179. https://doi.org/10.1061/(ASCE)0733-9402(1992)118:3(164)
5. Chacko, B., Balabaskaran, V., Tulapurkara, E. G., & Radha Krishna, H. C. (1994). Performance of S-cambered profiles with cut-off trailing edges. *Journal of Fluids Engineering Transactions*, *116*(3), 522–527. https://doi.org/10.1115/1.2910308
6. Garcia-Sagrado, A., & Hynes, T. (2011). Wall pressure sources near an airfoil trailing edge under turbulent boundary layers. *Journal of Fluids and Structures*, *30*(4), 3–34. https://doi.org/10.1016/j.jfluidstructs.2011.12.007
7. Guo, B., Wang, D. Z., Zhou, X., Shi, W. C., & Jing, F. M. (2019). Performance evaluation of a tidal current turbine with bidirectional symmetrical foils. *Water*, *12*(1), 22. https://doi.org/10.3390/w12010022
8. Huang, X., Albers, M., Meysonnat, P. S., Meinke, M., & Schröder, W. (2020). Analysis of the effect of freestream turbulence on dynamic stall of wind turbine blades. *International Journal of Heat and Fluid Flow*, *85*, 108668. https://doi.org/10.1016/j.ijheatfluidflow.2020.108668
9. Köktürk, T. (2005). *Design and performance analysis of a reversible axial flow fan* (Master's thesis). Graduate School of Natural and Applied Sciences, Middle East Technical University.
10. Li, J. Y., Guo, P. H., Xi, G., & Chen, W. W. (2011). Efficiency enhancement mechanisms of a new type of full reversible axial-flow fan. *Proceedings of the Institution of Mechanical Engineers, Part A: Journal of Power and Energy*, *225*(4), 467–480. https://doi.org/10.1177/0957650911399036
11. Ma, P. F., & Wang, J. (2017). An analysis on the flow characteristics of bi-directional axial-flow pump under reverse operation. *Proceedings of the Institution of Mechanical Engineers, Part A: Journal of Power and Energy*, *231*(3), 239–249. https://doi.org/10.1177/0957650917695447
12. Ma, P. F., Wang, J., & Li, H. (2014). Numerical analysis of pressure pulsation for a bidirectional pump under positive and reverse operation. *Advances in Mechanical Engineering*, *6*(8), 730280. https://doi.org/10.1155/2014/730280
13. Ma, P. F., Wang, J., & Wang, H. F. (2018). Investigation of performances and flow characteristics of two bi-directional pumps with different airfoil blades. *Science China Technological Sciences*, *61*(10), 1588–1599. https://doi.org/10.1007/s11431-017-9195-x
14. Madhusudn, R., Narayana, P. A. A., Balabaskaran, V., & Tulapurkara, E. G. (1994). Boundary layer studies over an S-blade. *Fluid Dynamics Research*, *14*(5), 241–258. https://doi.org/10.1016/0169-5983(94)90034-5
15. Matveev, K. I., Wheeler, M. P., & Xing, T. (2019). Numerical simulation of air ventilation and its suppression on inclined surface-piercing hydrofoils. *Ocean Engineering*, *175*, 251–261. https://doi.org/10.1016/j.oceaneng.2019.02.040
16. Meng, F., Yuan, S. Q., & Li, Y. J. (2018). Fluid–structure coupling analysis of impeller in unstable region for a reversible axial-flow pump device. *Advances in Mechanical Engineering*, *10*(3), 1–10. https://doi.org/10.1177/1687814017751762
17. Moisel, C., & Carolus, T. H. (2016). A facility for testing the aerodynamic and acoustic performance of bidirectional air turbines for ocean wave energy conversion. *Renewable Energy*, *86*, 1340–1352. https://doi.org/10.1016/j.renene.2015.09.062
18. Ohtake, T., Nakae, Y., & Motohashi, T. (2007). Nonlinearity of the aerodynamic characteristics of NACA0012 airfoil at low Reynolds numbers. *Journal of the Japan Society for Aeronautical and Space Sciences*, *55*(9), 439–445. https://doi.org/10.2322/jjsass.55.439
19. Oro, J. M. F., Díaz, K. M. A., Morros, C. S., & Ballesteros-Tajadura, R. (2009). Impact of the tip vortex on the passage flow structures of a jet fan with symmetric blades. *Proceedings of the Institution of Mechanical Engineers, Part A: Journal of Power and Energy*, *223*(2), 141–155. https://doi.org/10.1243/09576509JPE684
20. Premkumar, M., & Chatterjee, D. (2015). Computational analysis of flow over a cascade of S-shaped hydrofoil of fully reversible pump-turbine used in extracting tidal energy. *Renewable Energy*, *77*, 240–249. https://doi.org/10.1016/j.renene.2014.12.019

21. Premkumar, T. M., & Chatterjee, D. (2008). Numerical study of turbulent flow over an S-shaped hydrofoil. *Proceedings of the Institution of Mechanical Engineers, Part C: Journal of Mechanical Engineering Science*, *222*(9), 1717–1734. https://doi.org/10.1243/09544062JMES929

22. Premkumar, T. M., Kumar, P., & Chatterjee, D. (2014). Cavitation characteristics of S-blade used in fully reversible pump-turbine. *Journal of Fluids Engineering*, *136*(5), 051101. https://doi.org/10.1115/1.4026441

23. Ramachandran, R., Krishna, H. C., & Narayana, P. A. (1986). Cascade experiments over 'S' blade profiles. *Journal of Energy Engineering*, *112*(1), 37–50. https://doi.org/10.1061/(ASCE)0733-9402(1986)112:1(37)

24. Siemens Digital Industries Software. (2022). *Simcenter STAR-CCM+ user guide* (Version 17.04). Plano, TX: Siemens.

25. Spasic, Z., Jovanovic, M., & Bogdanovic-Jovanovic, J. (2018). Design and performance of low-pressure reversible axial fan with doubly curved profiles of blades. *Journal of Mechanical Science and Technology*, *32*(8), 3707–3712. https://doi.org/10.1007/s12206-018-0723-6

26. Spasic, Z., Jovanovic, M., Bogdanovic-Jovanovic, J., & Milanovic, S. (2020). Numerical investigation of the influence of the doubly curved blade profiles on the reversible axial fan characteristics. *Facta Universitatis Series: Mechanical Engineering*, *18*(1), 57–68. https://doi.org/10.22190/FUME171128002S

27. Spasic, Z. T., Milanovic, S., Sustersic, V. M., & Nikolic, B. D. (2012). Low-pressure reversible axial fan with straight profile blades and relatively high efficiency. *Thermal Science*, *16*(S2), 593–603. https://doi.org/10.2298/TSCI120503194S

28. Thakker, A., & Abdulhadi, R. (2008). The performance of Wells turbine under bi-directional airflow. *Renewable Energy*, *33*, 2467–2474. https://doi.org/10.1016/j.renene.2008.02.013

29. Tsuru, W., Kinoue, Y., Murakami, T., Sakaguchi, M., Shiomi, N., & Takao, M. (2023). Design method for a bidirectional ducted tidal turbine. *Journal of Aerospace Engineering*, *36*(2), 04025006. https://doi.org/10.1061/(ASCE)AS.1943-5525.0001591